

A Prototype Atom Interferometer to Detect Dark Matter and Gravitational Waves

C. F. A. Baynham^a, R. Hobson^a, O. Buchmüller, D. Evans,
L. Hawkins, L. Iannizzotto-Venezze, A. Josset, D. Lee,
E. Pasatembou, B. E. Sauer, M. R. Tarbutt, T. Walker;¹

O. Ennis, U. Chauhan, A. Brzakalik, S. Dey, S. Hedges^b, B. Stray^c,
M. Langlois^d, K. Bongs^e, T. Hird, S. Lellouch, M. Holynski;²

B. Bostwick^f, J. Chen, Z. Eyler, V. Gibson, T. L. Harte, C. C. Hsu,
M. Karzazi, C. Lu, B. Millward, J. Mitchell, N. Mouelle,
B. Panchumarthi^g, J. Scheper, U. Schneider, X. Su^h, Y. Tang,
K. Tkalčec, M. Zeunerⁱ, S. Zhang, Y. Zhi^j;³

^aLead authors who contributed equally to this work

^bPresent address: Nomad Atomics, 33 Elizabeth Street, Richmond, Victoria 3121, Australia

^cPresent address: Jet Propulsion Laboratory, California Institute of Technology, Pasadena, California 91109, USA

^dPresent address: Jet Propulsion Laboratory, California Institute of Technology, Pasadena, California 91109, USA

^ePresent address: Institute of Quantum Technologies, German Aerospace Center (DLR), Wilhelm-Runge-Straße 10, 89081 Ulm, Germany

^fPresent address: Kirchhoff-Institut für Physik, Universität Heidelberg, Im Neuenheimer Feld 227, 69120 Heidelberg, Germany

^gPresent address: Department of Physics & Astronomy, Northwestern University, 2145 Sheridan Road, Evanston, Illinois 60208-3112, United States

^hPresent address: Physikalisches Institut, Universität Tübingen, Auf der Morgenstelle 14, 72076 Tübingen, Germany

ⁱPresent address: Ludwig-Maximilians-Universität München, Geschwister-Scholl-Platz 1, 80539 München, Germany

^jPresent address: Department of Physics, University of Virginia, 382 McCormick Road, Charlottesville, VA 22904, USA

L. Badurina^k, A. Beniwal^l, D. Blas^m, J. Carlton, J. Ellis,
C. McCabe, G. Parish, D. Pathak Govardhan, V. Vaskonenⁿ; ⁴

T. Bowcock, K. Bridges, A. Carroll, J. Coleman, G. Elertas,
S. Hindley, C. Metelko, H. Throssell, J. N. Tinsley; ⁵

E. Bentine, M. Booth, D. Bortoletto, N. Callaghan, C. Foot,
C. Gomez-Monederro, K. Hughes, A. James, T. Leese, A. Lowe,
J. March-Russell, J. Sander, J. Schelfhout, I. Shipsey[†],
D. Weatherill, D. Wood; ⁶

S.N. Balashov, M.G. Bason, K. Hussain^o, H. Labiad, P. Majewski,
A.L. Marchant, D. Newbold, Z. Pan, Z. Tam, T.C. Thornton,
T. Valenzuela, M.G.D. van der Grinten, I. Wilmot; ⁷

K. Clarke, A. Vick⁸

¹Department of Physics, Blackett Laboratory, Imperial College London,
Prince Consort Road, London, SW7 2AZ, UK.

²Physics and Astronomy, University of Birmingham, Edgbaston,
Birmingham, B15 2TT, UK.

³Cavendish Laboratory, J J Thomson Avenue, University of Cambridge,
Cambridge, CB3 0HE, UK.

⁴Physics Department, King's College London, Strand, London,
WC2R 2LS, UK.

⁵Department of Physics, University of Liverpool, Merseyside, L69 7ZE,
UK.

⁶Department of Physics, University of Oxford, Parks Road, Oxford,
OX1 3PU, UK.

⁷Rutherford Appleton Laboratory, UKRI-STFC, Harwell Campus,
Didcot, OX11 0QX, UK.

⁸STFC Daresbury Laboratory, Warrington, WA4 4AD, UK.

^kPresent address: Walter Burke Institute for Theoretical Physics, California Institute of Technology, Pasadena, CA 91125, USA

^lPresent address: Intersect Australia, Sydney, Australia

^mPresent address: Institut de Física d'Altes Energies (IFAE), The Barcelona Institute of Science and Technology, Campus UAB, 08193 Bellaterra (Barcelona), Spain and Institució Catalana de Recerca i Estudis Avançats (ICREA), Passeig Lluís Companys 23, 08010 Barcelona, Spain

ⁿPresent address: Keemilise ja Bioloogilise Füüsika Instituut, Rävala pst. 10, 10143 Tallinn, Estonia

[†]Deceased

^oAlso at the University of Liverpool⁵

Abstract

The AION project has built a tabletop prototype of a single-photon long-baseline atom interferometer using the ^{87}Sr clock transition—a type of quantum sensor designed to search for dark matter and gravitational waves. Our prototype detector operates at the Standard Quantum Limit (SQL), producing a signal with no unexpected noise beyond atom shot noise. Importantly, the detector remains at the SQL even when additional laser phase noise is introduced, emulating conditions in a long-baseline detector such as AION or AEDGE where significant laser phase deviations will accumulate during long atom interrogation times. Our results mark a key milestone in extending atom interferometers to long baselines. Such interferometers can complement laser-interferometer gravitational wave detectors by accessing the mid-frequency gravitational wave band around 1 Hz, and can search for physics beyond the Standard Model.

The discovery of gravitational waves (GWs) by the LIGO and Virgo laser interferometer experiments [1] has opened a new window on the Universe, with prospects for breakthroughs in fundamental physics, astrophysics and cosmology. Just as observations of electromagnetic waves over a wide range of frequencies have provided insights into physical processes within and beyond our galaxy, as well as in the primordial Universe, it is expected that GW observations over a wide range of frequencies will offer complementary insights into an equally rich spectrum of phenomena. The operating terrestrial laser interferometer detectors, LIGO, Virgo and KAGRA, are sensitive to GWs at frequencies around 10^2 Hz [2–4], and the Laser Interferometer Space Antenna (LISA) experiment, now under construction, will be most sensitive to GWs with frequencies around 10^{-2} Hz [5], leaving unexplored an intermediate range of frequencies around 1 Hz.

Important sources of GWs in this frequency range are mergers of intermediate-mass black holes, heavier than those detected by ground-based laser interferometers, and lighter than those targeted by LISA. Such intermediate-mass black holes are thought to provide building blocks for the supermassive black holes [6] at the hearts of most galaxies, so measurements of their mergers using long-baseline atom interferometers [7, 8] could reveal how supermassive black holes are formed [9]. Further, observations of the slowly evolving inspiral stages of solar-mass mergers would be possible for days or weeks instead of seconds, enabling multi-messenger astronomy by pinpointing the locations of GW sources in the sky [10].

Atom interferometers, which employ lasers to split and recombine the wavefunctions of atoms, have optimal sensitivities to GWs with frequencies $\mathcal{O}(1)$ Hz [11, 12] and hence are well suited to explore the frequency gap between terrestrial and space-borne laser interferometers as seen in Figure 1. With the gradiometer configuration shown in Figure 2, a single-photon atom interferometer with a baseline ~ 1 km could achieve sufficient sensitivity to detect GWs [13, 14] with frequencies ~ 1 Hz that currently cannot be measured. Such detectors are also sensitive to theorized interactions between atomic constituents and bosonic dark matter fields with masses $\sim 10^{-15}$ eV [15].

Long-baseline atom interferometers are under development by the AION [11] and MAGIS [12] collaborations, and other projects worldwide [19], but realising the potential of these experiments will require overcoming many technical obstacles to reach the target sensitivity. One open question for these projects is whether the laser phase noise, which introduces noise on each individual atom interferometer that is orders of magnitude higher than the SQL (see Methods), will cancel sufficiently in the gradiometer configuration to reach the SQL. While the gradiometer principle has previously been demonstrated in experiments using ^{88}Sr [20] and ^{87}Rb [21, 22], in this work we quantify the extent of noise cancellation afforded by the scheme. We do this for the first time with the more demanding fermionic isotope ^{87}Sr , whose hyperfine structure and mHz-linewidth clock transition significantly complicate laser cooling and atom interferometry [23, 24]. Despite these challenges, ^{87}Sr is

a natural choice for gravitational-wave detection, thanks to its near-ideal properties as an atomic clock isotope [25] and 150 s excited-state lifetime [26]. These qualities are not shared by other candidate species such as ^{87}Rb or ^{88}Sr but are essential for very long baseline experiments, even extending to space-scale baselines [18].

We describe in this paper how the AION project has, for the first time, tested a gradiometer configuration in the laboratory using ^{87}Sr . We combine atomic clock technology with atom interferometry, forming two macroscopically separated interferometers interrogated by a common clock laser. Our prototype detector reaches the SQL even in the presence of arbitrarily high, induced laser phase noise, implying complete phase noise cancellation to within the measurement resolution of our experiment. While further work will be essential to demonstrate laser phase noise cancellation with

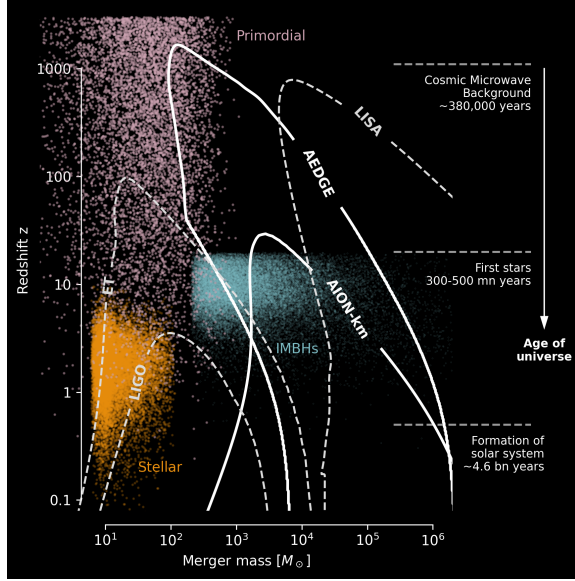


Fig. 1 The parameter space of black hole mergers probed by various GW detectors, both operational and planned. The horizontal axis gives the mass M of the black hole merger causing the GW, in units of the solar mass. The vertical axis is the distance to the GW source, expressed as the redshift z . The cyan dots are GW signals from a simulation of a one-year data sample of black hole mergers generated using a hierarchical model of the formation of supermassive black holes [6], the yellow dots are GW signals from a simulated sample of stellar mass black hole mergers, and the violet dots are GW signals from a hypothetical population of primordial black holes (see Methods for details). Also shown are the prospective sensitivities of different detectors, including laser-interferometer detectors [2, 5, 16] as well as AION-km [17] and AEDGE [18] atom-interferometer detectors with baselines of 1 km and 40 000 km respectively. This figure was inspired by the Cosmic Explorer proposal [16].

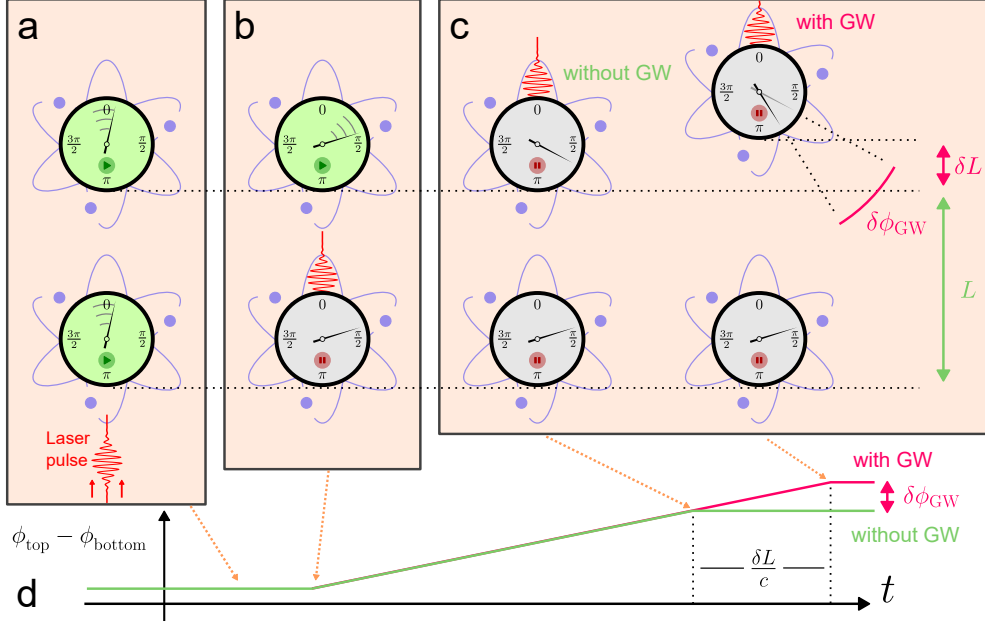


Fig. 2 An illustration of the detector’s sensitivity to gravitational waves. In the moments before the final $\pi/2$ beam splitter pulse (see Figure 3), the two atom interferometers can be treated as freely-falling atomic clocks (a) accruing phase at a rate ω_0 . The pulse halts this accrual of phase for the lower cloud, resulting in an accrual of differential phase (b, d) that continues until the pulse reaches the second cloud (c). In the proper frame of the bottom cloud (as pictured), the atoms are tidally displaced by a transient gravitational wave. This has the effect of delaying (or hastening) this second interaction, imparting (at leading order) a detectable differential phase of $\delta\phi_{\text{GW}} = \pm \frac{\delta L}{c} \omega_0$ [27]. Crucially, any phase noise due to the laser pulse itself is strongly suppressed in the differential measurement since it impacts both interferometers equally. The mechanism for sensitivity to dark matter (not pictured) is similar, but results from modulation of ω_0 instead of L —see Refs. [15, 28–31] for descriptions. This simplified picture neglects complications arising from other interferometer phases ϕ_{other} [12], the other pulses in the sequence [14, 32] and the choice of general relativistic gauge [27, 33].

larger atom numbers (for which the SQL is lower), and at longer baselines where wave-front propagation effects become relevant, our work verifies the principles underpinning long-baseline, single-photon atom interferometry, passing an important milestone on the road towards measurement of gravitational waves.

Analogously to the interference of light in a laser interferometer such as that used in the LIGO, Virgo and KAGRA experiments, atom interferometry relies on the interference of quantum matter waves. In the search for gravitational waves, both techniques probe a long baseline whose length in the proper detector frame is modulated by a gravitational wave, converting the variations in time-of-flight of light along this baseline to a variation of phase in an interference measurement—see Figure 2. For a discussion in a fully relativistic framework, see Refs. [27, 34]. In laser interferometers, the interference is between light beams that travel along different paths. In atom interferometers, the interference is in the wave functions of atoms that are manipulated by laser pulses to follow spatially-separated paths before recombination.

In a single-photon atom interferometer, the atomic wavefunction is manipulated using pulses of light that drive a single-photon transition in the atom, often referred to as a clock transition. For the pulse sequence shown in Figure 3, the phase of a single interferometer can be written in the simplified form

$$\phi = \int_{-\infty}^{\infty} \omega_0 g(t) dt + \phi_{\text{laser}} + \phi_{\text{other}}, \quad (1)$$

where ω_0 is the angular frequency of the atomic clock transition, ϕ_{laser} represents the total phase imprinted on the atoms due to the laser's phase during pulses, and ϕ_{other} comes from various sources such as static background gravitational or electromagnetic fields [12, 14, 33, 35], which do not play a role in the dark matter or gravitational wave detection. $g(t)$ is determined by the relative states of the interferometer's upper and lower arms, where

$$g(t) = \begin{cases} -1 & \text{for } t \text{ between the first beamsplitter pulse and the mirror pulse,} \\ +1 & \text{for } t \text{ between the mirror pulse and the final beamsplitter pulse,} \\ 0 & \text{otherwise.} \end{cases} \quad (2)$$

In long-baseline atom interferometry, a fundamental physics signal is generated by taking the difference in phase $\delta\phi = \phi_{\text{top}} - \phi_{\text{bottom}}$ between two atom interferometers separated by a long distance. To visualize the sensitivity of $\delta\phi$ to gravitational waves, the atom interferometers can be conceptualised as atomic clocks that are sensitive to small changes in the time taken for light to traverse the baseline [36]. The clocks “tick” while $g_{\text{top}}(t)$ and $g_{\text{bottom}}(t)$ are non-zero; these intervals are defined by the light pulse arrival times at each interferometer, so a modulation of the baseline L by a gravitational wave alters the time counted by the clocks. Alternatively, light dark matter may cause small oscillations of atomic energy levels, affecting the tick-rate ω_0 differently due to the time-delay between the two interferometers [15, 28, 29, 37]. An important technical advantage of taking a *differential* measurement is that the noise in the laser-induced phase ϕ_{laser} cancels in common-mode: without laser noise cancellation, it would be unfeasible to achieve the ultimate target phase resolution of $10^{-5} \text{ rad}/\sqrt{\text{Hz}}$ in the detector [11] even using extremely low-noise lasers (see Methods).

Our tabletop prototype of a long-baseline atom interferometer detector is illustrated in Figure 3. We operate a pair of crossed optical dipole traps containing clouds of fermionic ^{87}Sr atoms at a temperature of approximately $2 \mu\text{K}$, loaded from a narrow-linewidth magneto-optical trap (see Methods for details). After the two clouds are released into free fall, an ultrastable clock laser (described in Ref [38]) addresses the $^1\text{S}_0$ to $^3\text{P}_0$ optical clock transition. A first pulse (not shown) selects the slowest atoms from the falling clouds, and a sequence of three pulses then splits, reflects, and recombines the selected atoms to create two simultaneous Mach-Zehnder atom interferometers [39]. After the first beam-splitter pulse, we apply an additional, horizontal laser pulse, off-resonant from the $^1\text{S}_0$ to $^3\text{P}_1$ transition, to induce a controllable Stark shift ϕ_{Stark} to just one of the interferometers (see Methods). The same Stark-shifting

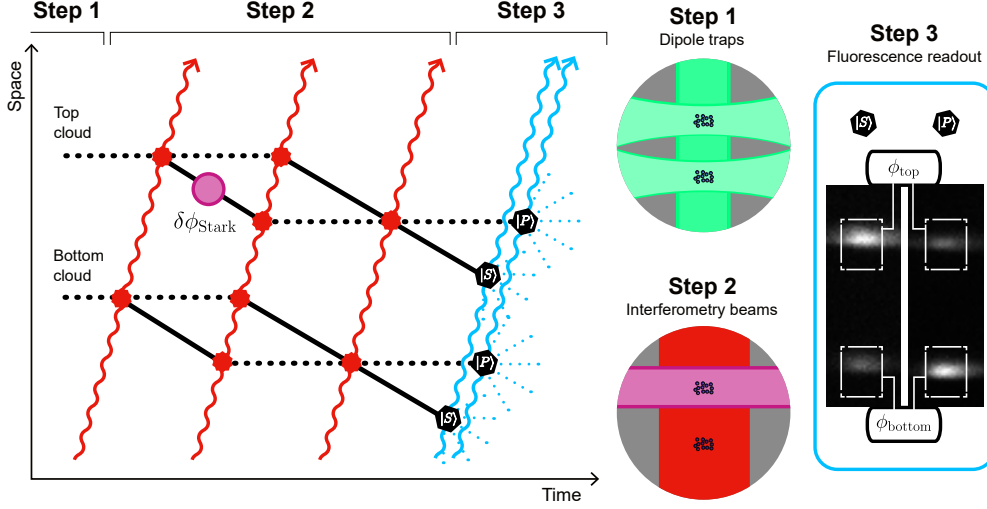


Fig. 3 Overview of steps in the experiment. (*Main figure, left*) Spacetime diagram of the paths taken by the arms of each interferometer. Clock pulses (red) create a superposition of 1S_0 (solid) and 3P_0 (dotted) atomic states following both paths. For simplicity, we do not the free-fall of the atoms. (*Step 1*) Two clouds of ^{87}Sr atoms are confined, cooled and then released from crossed optical traps (green). (*Step 2*) An ultrastable clock laser (red) interrogates both clouds. An additional beam (purple) applies a bias phase shift ϕ_{Stark} to just the top cloud, inducing a static, controllable differential phase between the two atom interferometers. To evaluate the noise rejection of the differential scheme [28], we inject randomised, artificial laser phase steps in the second and third laser pulses to emulate the effect of laser noise between pulses. (*Step 3*) Their interference is measured by reading out the atoms' states via a fluorescence measurement of the ground and excited states. The fluorescence images shown here had an excitation fraction of 20 % in the top cloud and 62 % in the bottom. See Methods for details of all these steps.

pulse is applied in every shot of the experiment, biasing the phase offset between the interferometers to aid the data analysis.

To gather the datasets presented in Figure 4, we scan the relative phases of the three clock pulses applied to both atom interferometers. Figure 4a shows the typical interference fringes we obtain. Using a π -pulse duration of $40\mu\text{s}$ and a free-fall time of $T = 100\mu\text{s}$ between pulses, an interferometer contrast of $\sim 80\%$ is observed. In order to simulate the effect of laser phase noise on a long-baseline atom interferometer, for one of the datasets we inject randomised phase steps to the clock laser between pulses of the atom interferometer sequence. This simulates the effect of laser phase error accumulated during the sequence, although it neglects its effect on the fidelity of mirror pulses. This is a reasonable representation of a long-baseline detector, since laser noise will be integrated over drop times of many seconds [11], amplifying its impact relative to our short sequence of $100\mu\text{s}$ (see Methods for a calculation). The resulting individual interference fringes are shown in the lower panel of Figure 4a, and are completely obscured by the injected noise. However, the differential phase $\delta\phi$ of the two interferometers can still be recovered with high fidelity via the Lissajous correlation plot (Figure 4b) [40].

To measure the impact of laser noise on the stability of the differential phase measurement, we compare measurements with the same applied differential phase ϕ_{Stark} ,

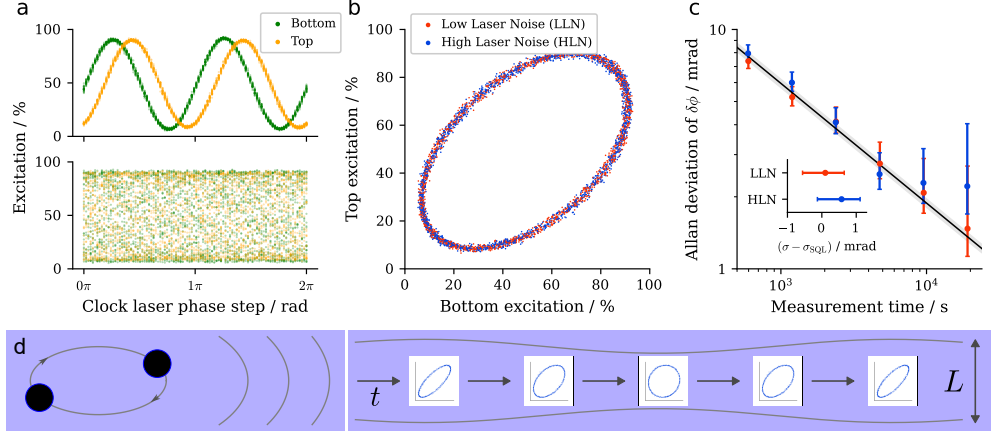


Fig. 4 (a) Clock atom interferometry fringes in the top and bottom atom clouds with a fixed Stark shift ϕ_{Stark} applied to the top cloud. The lower (upper) plot shows the fringes with (without) the addition of artificial laser noise (see Methods for details). (b) A correlation plot—or Lissajous figure—of the top and bottom atom interferometer signals, with (blue) and without (red) added laser noise. Despite the entirely obscured interferometer fringes, the differential measurement rejects laser noise, recovering a clean ellipse. (c) Overlapping Allan deviations of $\delta\phi$ calculated from 112 independent ellipse fits to consecutive bins of 100 shots each, comprising a total of 11 200 interferometer samples taken over 18.6 h. Using absorption spectroscopy (see Methods), we measure 1280(130) in the top trap and 1600(160) atoms in the bottom trap, forming the basis of our estimate of the Standard Quantum Limit (SQL, black). (c inset) The standard deviations σ of the differential phase measurements for the Low Laser Noise (LLN) and High Laser Noise (HLN) datasets are consistent with the SQL. (d) An illustration of how a passing low-frequency gravitational wave would modify the shape of the ellipse in the Lissajous figure: a gravitational wave would modulate $\delta\phi$ as the second derivative of the strain [14]. While this picture of slowly-distorted ellipses is accurate in the limit of low-frequency GWs, it would not be accurate for mid-band GWs, which would cause phase fluctuations that are too fast to be tracked by the ellipse fits. In the real detector, more complex data analysis techniques and experimental schemes will therefore be required [41, 42].

but with different levels of applied laser noise. We gather a “Low Laser Noise (LLN)” dataset in which only the intrinsic noise of the cavity-stabilized laser is present and a “High Laser Noise (HLN)” dataset with several radians of laser phase noise artificially added to each shot. For each of the two datasets, we extract a time-series of differential phases $\delta\phi(t_i)$ through least-squares fitting of ellipses [43] to a series of data bins, with each bin containing 100 individual shots of the interferometers. Figure 4c shows the Allan variance [44] of these datasets; despite laser noise that completely obscures individual interferometer fringes, we observe no statistically significant increase in noise beyond the SQL in the differential phase $\delta\phi$. The SQL noise level was simulated based on an independent measurement of atom number, detailed in Methods.

To quantify this rejection, we use Bayesian analysis to infer the noise levels of the measured $\delta\phi$ time-series in both cases. We determine that the standard deviations σ of $\delta\phi$ are consistent with the SQL in both the LLN and the HLN dataset, with $\sigma_{\text{LLN}} - \sigma_{\text{SQL}} = 0.10^{+0.55}_{-0.66}$ mrad and $\sigma_{\text{HLN}} - \sigma_{\text{SQL}} = 0.57^{+0.54}_{-0.70}$ mrad (Figure 4c, inset), for an SQL determined by the 1280(130) and 1600(160) atoms observed in the top and bottom traps (see Methods). Crucially, we observe no statistically significant

increase in noise despite the addition of maximal laser noise in the HLN dataset, with $\sigma_{\text{HLN}} - \sigma_{\text{LLN}} = 0.47^{+0.72}_{-0.77}$ mrad.

The successful integration of clock transition techniques with atom interferometry is an important milestone on the path towards their joint implementation in sensitive quantum sensors with applications in fundamental physics. These include not only the detection of gravitational waves that we have highlighted, but also the search for the interactions of dark matter with atoms [15] and tests of equivalence principles [45, 46]. The construction of long-baseline detectors will also spur quantum sensing advancements with applications in navigation, geodesy, and resource exploration (see, e.g., Ref. [22]).

We have demonstrated at the laboratory scale the principle behind laser noise cancellation for the much longer baseline devices required to achieve high sensitivity to gravitational waves or dark matter [11, 12, 17]. There are, however, many further technical hurdles to be overcome before such a long-baseline detector can be realised. These include the development of more intense sources of cold atoms, the extension to longer baselines while controlling associated systematic shifts [12, 35], the demonstration of multiple momentum transfers to the atoms by the laser used to manipulate them [47] and the use of squeezed atomic states [48]. All of these are the subjects of R&D programmes by the AION and MAGIS teams, as well as other groups within the international Terrestrial Very Long Baseline Atom Interferometry Protocol Collaboration [19]. Nevertheless, the experimental techniques presented here open up exciting new avenues for scientific exploration that range from probing the fundamental laws that govern our Universe to enhancing quantum sensors. As we continue to refine these techniques, the next generation of atom interferometers offers the prospect of a significant leap forward in our ability to observe and understand the subtle forces that shape our world.

References

- [1] Abbott, B.P., *et al.*: Observation of Gravitational Waves from a Binary Black Hole Merger. *Phys. Rev. Lett.* **116**(6), 061102 (2016) <https://doi.org/10.1103/PhysRevLett.116.061102> [arXiv:1602.03837](https://arxiv.org/abs/1602.03837) [gr-qc]
- [2] Aasi, J., *et al.*: Advanced LIGO. *Class. Quant. Grav.* **32**, 074001 (2015) <https://doi.org/10.1088/0264-9381/32/7/074001> [arXiv:1411.4547](https://arxiv.org/abs/1411.4547) [gr-qc]
- [3] Acernese, F., *et al.*: Advanced Virgo: a second-generation interferometric gravitational wave detector. *Class. Quant. Grav.* **32**(2), 024001 (2015) <https://doi.org/10.1088/0264-9381/32/2/024001> [arXiv:1408.3978](https://arxiv.org/abs/1408.3978) [gr-qc]
- [4] Aso, Y., Michimura, Y., Somiya, K., Ando, M., Miyakawa, O., Sekiguchi, T., Tatum, D., Yamamoto, H.: Interferometer design of the KAGRA gravitational wave detector. *Phys. Rev. D* **88**(4), 043007 (2013) <https://doi.org/10.1103/PhysRevD.88.043007> [arXiv:1306.6747](https://arxiv.org/abs/1306.6747) [gr-qc]
- [5] Amaro-Seoane, P., *et al.*: Laser Interferometer Space Antenna (2017)

[arXiv:1702.00786](#) [astro-ph.IM]

- [6] Ellis, J., Fairbairn, M., Urrutia, J., Vaskonen, V.: What is the origin of the JWST SMBHs? (2024) [arXiv:2410.24224](#) [astro-ph.CO]
- [7] Abend, S., *et al.*: Terrestrial Very-Long-Baseline Atom Interferometry: Workshop Summary (2023). <https://doi.org/10.1116/5.0185291>
- [8] Abdalla, A., *et al.*: Terrestrial Very-Long-Baseline Atom Interferometry: Summary of the Second Workshop, arXiv:2412.14960 (2024)
- [9] Ellis, J., Fairbairn, M., Urrutia, J., Vaskonen, V.: Probing Supermassive Black Hole Seed Scenarios with Gravitational-wave Measurements. *Astrophys. J.* **964**(1), 11 (2024) <https://doi.org/10.3847/1538-4357/ad27d5> [arXiv:2312.02983](#) [astro-ph.CO]
- [10] Baum, S., Bogorad, Z., Graham, P.W.: Gravitational wave measurement in the mid-band with atom interferometers. *Journal of Cosmology and Astroparticle Physics* **2024**(05), 027 (2024) <https://doi.org/10.1088/1475-7516/2024/05/027> . Accessed 2025-02-27
- [11] Badurina, L., Bentine, E., Blas, D., Bongs, K., Bortoletto, D., Bowcock, T., Bridges, K., Bowden, W., Buchmueller, O., Burrage, C., Coleman, J., Elertas, G., Ellis, J., Foot, C., Gibson, V., Hahnelt, M.G., Harte, T., Hedges, S., Hobson, R., Holynski, M., Jones, T., Langlois, M., Lellouch, S., Lewicki, M., Maiolino, R., Majewski, P., Malik, S., March-Russell, J., McCabe, C., Newbold, D., Sauer, B., Schneider, U., Shipsey, I., Singh, Y., Uchida, M.A., Valenzuela, T., Grinten, M.V.D., Vaskonen, V., Vosseveld, J., Weatherill, D., Wilmut, I.: AION: An atom interferometer observatory and network. *Journal of Cosmology and Astroparticle Physics* **2020** (2020) <https://doi.org/10.1088/1475-7516/2020/05/011>
- [12] Abe, M., Adamson, P., Borceian, M., Bortoletto, D., Bridges, K., Carman, S.P., Chattopadhyay, S., Coleman, J., Curfman, N.M., DeRose, K., Deshpande, T., Dimopoulos, S., Foot, C.J., Frisch, J.C., Garber, B.E., Geer, S., Gibson, V., Glick, J., Graham, P.W., Hahn, S.R., Harnik, R., Hawkins, L., Hindley, S., Hogan, J.M., Jiang, Y., Kasevich, M.A., Kellett, R.J., Kiburg, M., Kovachy, T., Lykken, J.D., March-Russell, J., Mitchell, J., Murphy, M., Nantel, M., Nobrega, L.E., Plunkett, R.K., Rajendran, S., Rudolph, J., Sachdeva, N., Sardari, M., Santucci, J.K., Schwartzman, A.G., Shipsey, I., Swan, H., Valerio, L.R., Vasonis, A., Wang, Y., Wilkason, T.: Matter-wave Atomic Gradiometer Interferometric Sensor (MAGIS-100). *Quantum Sci. Technol.* **6**(4), 044003 (2021) <https://doi.org/10.1088/2058-9565/abf719>
- [13] Yu, N., Tinto, M.: Gravitational wave detection with single-laser atom interferometers. *General Relativity and Gravitation* **43**(7), 1943–1952 (2011) <https://doi.org/10.1007/s10714-010-1055-8> . Accessed 2025-01-23

- [14] Graham, P.W., Hogan, J.M., Kasevich, M.A., Rajendran, S.: New Method for Gravitational Wave Detection with Atomic Sensors. *Phys. Rev. Lett.* **110**(17), 171102 (2013) <https://doi.org/10.1103/PhysRevLett.110.171102> . Accessed 2020-01-05
- [15] Arvanitaki, A., Graham, P.W., Hogan, J.M., Rajendran, S., Van Tilburg, K.: Search for light scalar dark matter with atomic gravitational wave detectors. *Phys. Rev. D* **97**(7), 075020 (2018) <https://doi.org/10.1103/PhysRevD.97.075020> [arXiv:1606.04541](https://arxiv.org/abs/1606.04541) [hep-ph]
- [16] Evans, M., Corsi, A., Afle, C., Ananyeva, A., Arun, K.G., Ballmer, S., Bandyopadhyay, A., Barsotti, L., Baryakhtar, M., Berger, E., Berti, E., Biscoveanu, S., Borhanian, S., Broekgaarden, F., Brown, D.A., Cahillane, C., Campbell, L., Chen, H.-Y., Daniel, K.J., Dhani, A., Driggers, J.C., Effler, A., Eisenstein, R., Fairhurst, S., Feicht, J., Fritschel, P., Fulda, P., Gupta, I., Hall, E.D., Hammond, G., Hannuksela, O.A., Hansen, H., Haster, C.-J., Kacanja, K., Kamai, B., Kashyap, R., Key, J.S., Khadkikar, S., Kontos, A., Kuns, K., Landry, M., Landry, P., Lantz, B., Li, T.G.F., Lovelace, G., Mandic, V., Mansell, G.L., Martynov, D., McCuller, L., Miller, A.L., Nitz, A.H., Owen, B.J., Palomba, C., Read, J., Phurailatpam, H., Reddy, S., Richardson, J., Rollins, J., Romano, J.D., Sathyaprakash, B.S., Schofield, R., Shoemaker, D.H., Sigg, D., Singh, D., Slagmolen, B., Sledge, P., Smith, J., Soares-Santos, M., Strunk, A., Sun, L., Tanner, D., Son, L.A.C.v., Vitale, S., Willke, B., Yamamoto, H., Zucker, M.: Cosmic Explorer: A Submission to the NSF MPSAC ngGW Subcommittee. *arXiv*. [arXiv:2306.13745](https://arxiv.org/abs/2306.13745) [astro-ph] (2023). <https://doi.org/10.48550/arXiv.2306.13745> . [http://arxiv.org/abs/2306.13745](https://arxiv.org/abs/2306.13745) Accessed 2025-02-26
- [17] Badurina, L., Buchmueller, O., Ellis, J., Lewicki, M., McCabe, C., Vaskonen, V.: Prospective sensitivities of atom interferometers to gravitational waves and ultralight dark matter. *Phil. Trans. A. Math. Phys. Eng. Sci.* **380**(2216), 20210060 (2021) <https://doi.org/10.1098/rsta.2021.0060> [arXiv:2108.02468](https://arxiv.org/abs/2108.02468) [gr-qc]
- [18] El-Neaj, Y.A., *et al.*: AEDGE: Atomic Experiment for Dark Matter and Gravity Exploration in Space. *EPJ Quant. Technol.* **7**, 6 (2020) <https://doi.org/10.1140/epjqt/s40507-020-0080-0> [arXiv:1908.00802](https://arxiv.org/abs/1908.00802) [gr-qc]
- [19] Memorandum of Understanding for the Terrestrial Very Long Baseline Atom Interferometer Study. <https://indico.cern.ch/event/1369392/attachments/2789312/5096609/TVLBAI%20Study%20MOU%20%20Final%20.pdf>. Accessed: 2024-11-11
- [20] Hu, L., Poli, N., Salvi, L., Tino, G.M.: Atom Interferometry with the Sr Optical Clock Transition. *Phys. Rev. Lett.* **119**(26), 263601 (2017) <https://doi.org/10.1103/PhysRevLett.119.263601>
- [21] Snadden, M.J., McGuirk, J.M., Bouyer, P., Haritos, K.G., Kasevich, M.A.: Measurement of the Earth's Gravity Gradient with an Atom Interferometer-Based

- Gravity Gradiometer. *Physical Review Letters* **81**(5), 971–974 (1998) <https://doi.org/10.1103/PhysRevLett.81.971> . Publisher: American Physical Society. Accessed 2025-02-27
- [22] Stray, B., Lamb, A., Kaushik, A., Vovrosh, J., Rodgers, A., Winch, J., Hayati, F., Boddice, D., Stabrawa, A., Niggebaum, A., *et al.*: Quantum sensing for gravity cartography. *Nature* **602**(7898), 590–594 (2022)
 - [23] Mukaiyama, T., Katori, H., Ido, T., Li, Y., Kuwata-Gonokami, M.: Recoil-limited laser cooling of ^{87}Sr atoms near the Fermi temperature. *Phys. Rev. Lett.* **90**(11), 113002 (2003) <https://doi.org/10.1103/PhysRevLett.90.113002>
 - [24] Akatsuka, T., Takahashi, T., Katori, H.: Optically guided atom interferometer tuned to magic wavelength. *Applied Physics Express* **10**(11), 112501 (2017) <https://doi.org/10.7567/APEX.10.112501> . Publisher: IOP Publishing. Accessed 2025-02-26
 - [25] Aeppli, A., Kim, K., Warfield, W., Safronova, M.S., Ye, J.: Clock with 8×10^{-19} systematic uncertainty. *Phys. Rev. Lett.* **133**, 023401 (2024) <https://doi.org/10.1103/PhysRevLett.133.023401>
 - [26] Lu, X.-T., Guo, F., Liu, Y.-Y., Xia, J.-J., Zhao, G.-D., Chen, Y.-X., Wang, Y.-B., Lu, B.-Q., Chang, H.: Determining the lifetime of the $5s5p\ ^3P_0^o$ metastable state in ^{87}Sr from the electric dipole matrix element. *Physical Review Applied* **21**(2), 024042 (2024) <https://doi.org/10.1103/PhysRevApplied.21.024042> . Publisher: American Physical Society. Accessed 2025-03-25
 - [27] Badurina, L., Du, Y., Lee, V.S.H., Wang, Y., Zurek, K.M.: Signatures of Linearized Gravity in Atom Interferometers: a Simplified Computational Framework (2024). <https://arxiv.org/abs/2409.03828>
 - [28] Graham, P.W., Kaplan, D.E., Mardon, J., Rajendran, S., Terrano, W.A.: Dark Matter Direct Detection with Accelerometers. *Phys. Rev. D* **93**(7), 075029 (2016) <https://doi.org/10.1103/PhysRevD.93.075029> [arXiv:1512.06165](https://arxiv.org/abs/1512.06165) [hep-ph]
 - [29] Badurina, L., Blas, D., McCabe, C.: Refined ultralight scalar dark matter searches with compact atom gradiometers. *Phys. Rev. D* **105**(2), 023006 (2022) <https://doi.org/10.1103/PhysRevD.105.023006> [arXiv:2109.10965](https://arxiv.org/abs/2109.10965) [astro-ph.CO]
 - [30] Badurina, L., Beniwal, A., McCabe, C.: Super-Nyquist ultralight dark matter searches with broadband atom gradiometers. *Phys. Rev. D* **108**(8), 083016 (2023) <https://doi.org/10.1103/PhysRevD.108.083016> [arXiv:2306.16477](https://arxiv.org/abs/2306.16477) [hep-ph]
 - [31] Blas, D., Carlton, J., McCabe, C.: Massive graviton dark matter searches with long-baseline atom interferometers (2024) [arXiv:2412.14282](https://arxiv.org/abs/2412.14282) [hep-ph]
 - [32] Graham, P.W., Hogan, J.M., Kasevich, M.A., Rajendran, S.: Resonant mode for

- gravitational wave detectors based on atom interferometry. *Physical Review D* **94**, 104022 (2016) <https://doi.org/10.1103/PhysRevD.94.104022>
- [33] Dimopoulos, S., Graham, P.W., Hogan, J.M., Kasevich, M.A.: General relativistic effects in atom interferometry. *Physical Review D* **78**, 042003 (2008) <https://doi.org/10.1103/PhysRevD.78.042003>
- [34] Dimopoulos, S., Graham, P.W., Hogan, J.M., Kasevich, M.A.: General Relativistic Effects in Atom Interferometry. *Phys. Rev. D* **78**, 042003 (2008) <https://doi.org/10.1103/PhysRevD.78.042003> [arXiv:0802.4098](https://arxiv.org/abs/0802.4098) [hep-ph]
- [35] Hogan, J.M., Johnson, D.M.S., Dickerson, S., Kovachy, T., Sugarbaker, A., Chiow, S.-w., Graham, P.W., Kasevich, M.A., Saif, B., Rajendran, S., Bouyer, P., Seery, B.D., Feinberg, L., Keski-Kuha, R.: An atomic gravitational wave interferometric sensor in low earth orbit (AGIS-LEO). *General Relativity and Gravitation* **43**(7), 1953–2009 (2011) <https://doi.org/10.1007/s10714-011-1182-x>. Accessed 2025-02-27
- [36] Norcia, M.A., Cline, J.R.K., Thompson, J.K.: Role of atoms in atomic gravitational-wave detectors. *Physical Review A* **96**(4), 042118 (2017) <https://doi.org/10.1103/PhysRevA.96.042118>. Publisher: American Physical Society. Accessed 2025-03-03
- [37] Bongs, K., Launay, R., Kasevich, M.A.: High-order inertial phase shifts for time-domain atom interferometers. *Applied Physics B* **84**(4), 599–602 (2006) <https://doi.org/10.1007/s00340-006-2397-5>. Accessed 2025-03-03
- [38] Stray, B., Ennis, O., Hedges, S., Dey, S., Langlois, M., Bongs, K., Lellouch, S., Holynski, M., Bostwick, B., Chen, J., Eyler, Z., Gibson, V., Harte, T.L., Hsu, C.C., Karzazi, M., Mitchell, J., Mouelle, N., Schneider, U., Tang, Y., Tkalec, K., Zhi, Y., Clarke, K., Vick, A., Bridges, K., Coleman, J., Elert, G., Hawkins, L., Hindley, S., Hussain, K., Metelko, C., Throssell, H., Baynham, C.F.A., Buchmüller, O., Evans, D., Hobson, R., Iannizzotto-Venezze, L., Josset, A., Pasatembou, E., Sauer, B.E., Tarbutt, M.R., Badurina, L., Beniwal, A., Blas, D., Carlton, J., Ellis, J., McCabe, C., Bentine, E., Booth, M., Bortoletto, D., Foot, C., Gómez-Monedero Castellanos, C.M., Hird, T., Hughes, K., James, A., Lowe, A., March-Russell, J., Schelfhout, J., Shipsey, I., Weatherill, D., Wood, D., Balashov, S., Bason, M.G., Boehm, J., Courthold, M., Grinten, M., Majewski, P., Marchant, A.L., Newbold, D., Pan, Z., Tam, Z., Valenzuela, T., Wilmut, I.: Centralized design and production of the ultra-high vacuum and laser-stabilization systems for the AION ultra-cold strontium laboratories. *AVS Quantum Science* **6**(1), 014409 (2024) <https://doi.org/10.1116/5.0172731>. Accessed 2024-12-18
- [39] Kasevich, M., Chu, S.: Atomic interferometry using stimulated Raman transitions. *Phys. Rev. Lett.* **67**(2), 181 (1991)
- [40] Foster, G.T., Fixler, J.B., McGuirk, J.M., Kasevich, M.A.: Method of phase

- extraction between coupled atom interferometers using ellipse-specific fitting. *Optics Letters* **27**(11), 951 (2002) <https://doi.org/10.1364/OL.27.000951>
- [41] Wigley, P.B., Hardman, K.S., Freier, C., Everitt, P.J., Legge, S., Manju, P., Close, J.D., Robins, N.P.: Readout-delay-free Bragg atom interferometry using overlapped spatial fringes. *Physical Review A* **99**(2), 023615 (2019) <https://doi.org/10.1103/PhysRevA.99.023615> . Publisher: American Physical Society. Accessed 2025-03-03
- [42] Sugarbaker, A., Dickerson, S.M., Hogan, J.M., Johnson, D.M.S., Kasevich, M.A.: Enhanced Atom Interferometer Readout through the Application of Phase Shear. *Physical Review Letters* **111**(11), 113002 (2013) <https://doi.org/10.1103/PhysRevLett.111.113002> . Publisher: American Physical Society. Accessed 2025-03-03
- [43] Foster, G.T., Fixler, J.B., McGuirk, J.M., Kasevich, M.A.: Method of phase extraction between coupled atom interferometers using ellipse-specific fitting. *Opt. Lett.* **27**(11), 951–953 (2002) <https://doi.org/10.1364/OL.27.000951>
- [44] Allan, D.W.: Statistics of atomic frequency standards. *Proceedings of the IEEE* **54**(2), 221–230 (1966)
- [45] Asenbaum, P., Overstreet, C., Kim, M., Curti, J., Kasevich, M.A.: Atom-Interferometric Test of the Equivalence Principle at the 10^{-12} Level. *Physical Review Letters* **125**(19), 191101 (2020) <https://doi.org/10.1103/PhysRevLett.125.191101> . Publisher: American Physical Society. Accessed 2021-08-12
- [46] Tarallo, M.G., Mazzoni, T., Poli, N., Sutyrin, D.V., Zhang, X., Tino, G.M.: Test of Einstein Equivalence Principle for 0-Spin and Half-Integer-Spin Atoms: Search for Spin-Gravity Coupling Effects. *Physical Review Letters* **113**(2), 023005 (2014) <https://doi.org/10.1103/PhysRevLett.113.023005> . Publisher: American Physical Society. Accessed 2025-03-03
- [47] Rudolph, J., Wilkason, T., Nantel, M., Swan, H., Holland, C.M., Jiang, Y., Garber, B.E., Carman, S.P., Hogan, J.M.: Large Momentum Transfer Clock Atom Interferometry on the 689 nm Intercombination Line of Strontium. *Physical Review Letters* **124**(8), 083604 (2020) <https://doi.org/10.1103/PhysRevLett.124.083604> . Publisher: American Physical Society. Accessed 2022-10-05
- [48] Corgier, R., Malitesta, M., Sidorenkov, L.A., Santos, F.P.D., Rosi, G., Tino, G.M., Smerzi, A., Salvi, L., Pezzè, L.: Squeezing-enhanced accurate differential sensing under large phase noise. *arXiv*. arXiv:2501.18256 [quant-ph] (2025). <https://doi.org/10.48550/arXiv.2501.18256> . <http://arxiv.org/abs/2501.18256> Accessed 2025-02-26
- [49] Pasatembou, E., Baynham, C.F.A., Buchmüller, O., Evans, D., Hobson, R., Iannizzotto Venezzè, L., Josset, A.: Progress toward ultra-cold Sr for the AION

- project—A red MOT and an optical-heterodyne diagnostic tool for injection-locked laser diodes. *AVS Quantum Science* **6**(1), 014408 (2024) <https://doi.org/10.1116/5.0180043> . Accessed 2024-12-18
- [50] Yang, T., Pandey, K., Pramod, M.S., Leroux, F., Kwong, C.C., Hajiyeve, E., Chia, Z.Y., Fang, B., Wilkowski, D.: A high flux source of cold strontium atoms. *The European Physical Journal D* **69**(10), 226 (2015) <https://doi.org/10.1140/epjd/e2015-60288-y> . Accessed 2020-09-06
 - [51] Snigirev, S., Park, A.J., Heinz, A., Bloch, I., Blatt, S.: Fast and dense magneto-optical traps for strontium. *Physical Review A* **99**(6), 063421 (2019) <https://doi.org/10.1103/PhysRevA.99.063421> . Accessed 2020-02-14
 - [52] Le Gouët, J., Mehlstäubler, T.E., Kim, J., Merlet, S., Clairon, A., Landragin, A., Pereira Dos Santos, F.: Limits to the sensitivity of a low noise compact atomic gravimeter. *Applied Physics B* **92**(2), 133–144 (2008) <https://doi.org/10.1007/s00340-008-3088-1> . Accessed 2025-02-27
 - [53] Steck, D.A.: Quantum and Atom Optics, 0.16.2 edn. Online, <http://steck.us/teaching> (2024)
 - [54] Numata, K., Kemery, A., Camp, J.: Thermal-Noise Limit in the Frequency Stabilization of Lasers with Rigid Cavities. *Physical Review Letters* **93**(25), 1–4 (2004) <https://doi.org/10.1103/PhysRevLett.93.250602>
 - [55] Oelker, E., Hutson, R.B., Kennedy, C.J., Sonderhouse, L., Bothwell, T., Goban, A., Kedar, D., Sanner, C., Robinson, J.M., Marti, G.E., Matei, D.G., Legero, T., Giunta, M., Holzwarth, R., Riehle, F., Sterr, U., Ye, J.: Demonstration of 4.8×10^{-17} stability at 1 s for two independent optical clocks. *Nature Photonics* **13**(10), 714–719 (2019) <https://doi.org/10.1038/s41566-019-0493-4> . Accessed 2020-02-17
 - [56] Jördens, R., Nadlinger, D., Harty, T., Slichter, D., Ballance, C., Lam, J., Maka, S., Wodey, E., Ho, H., Britton, J., et al.: ARTIQ. Online at: <https://m-labs.hk/artiq> (2023)
 - [57] Baynham, C.: Supporting data for “A Prototype Atom Interferometer to Detect Dark Matter and Gravitational Waves”. Zenodo (2025). <https://doi.org/10.5281/zenodo.15166670>
 - [58] Hueck, K., Luick, N., Sobirey, L., Siegl, J., Lompe, T., Moritz, H., Clark, L.W., Chin, C.: Calibrating high intensity absorption imaging of ultracold atoms. *Optics Express* **25**(8), 8670–8679 (2017) <https://doi.org/10.1364/OE.25.008670> . Publisher: Optica Publishing Group. Accessed 2025-03-07
 - [59] Kluge, H.-J., Sauter, H.: Levelcrossing experiments in the first excited $1P_1$ states of the alkaline earths. *Zeitschrift für Physik* **270**(4), 295–309 (1974) <https://doi.org/10.1007/BF01171111>

[org/10.1007/BF01677766](https://doi.org/10.1007/BF01677766) . Accessed 2025-03-07

- [60] Nagel, S.B., Mickelson, P.G., Saenz, A.D., Martinez, Y.N., Chen, Y.C., Killian, T.C., Pellegrini, P., Côté, R.: Photoassociative Spectroscopy at Long Range in Ultracold Strontium. *Physical Review Letters* **94**(8), 083004 (2005) <https://doi.org/10.1103/PhysRevLett.94.083004> . Publisher: American Physical Society. Accessed 2025-03-07
- [61] Abril-Pla, O., Andreani, V., Carroll, C., Dong, L., Fannesbeck, C.J., Kochurov, M., Kumar, R., Lao, J., Luhmann, C.C., Martin, O.A., Osthege, M., Vieira, R., Wiecki, T., Zinkov, R.: Pymc: a modern, and comprehensive probabilistic programming framework in python. *PeerJ Computer Science* **9** (2023) <https://doi.org/10.7717/peerj-cs.1516>
- [62] Hild, S., *et al.*: Sensitivity Studies for Third-Generation Gravitational Wave Observatories. *Class. Quant. Grav.* **28**, 094013 (2011) <https://doi.org/10.1088/0264-9381/28/9/094013> [arXiv:1012.0908](https://arxiv.org/abs/1012.0908) [gr-qc]
- [63] Badurina, L., Gibson, V., McCabe, C., Mitchell, J.: Ultralight dark matter searches at the sub-Hz frontier with atom multigradiometry. *Phys. Rev. D* **107**(5), 055002 (2023) <https://doi.org/10.1103/PhysRevD.107.055002> [arXiv:2211.01854](https://arxiv.org/abs/2211.01854) [hep-ph]
- [64] Carlton, J., Gibson, V., Kovachy, T., McCabe, C., Mitchell, J.: Characterizing atmospheric gravity gradient noise for vertical atom interferometers. *Phys. Rev. D* **111**(8), 082003 (2025) <https://doi.org/10.1103/PhysRevD.111.082003> [arXiv:2412.05379](https://arxiv.org/abs/2412.05379) [gr-qc]
- [65] Raidal, M., Vaskonen, V., Veermäe, H.: In: Byrnes, C., Franciolini, G., Harada, T., Pani, P., Sasaki, M. (eds.) *Formation of primordial black hole binaries and their merger rates*, (2024)
- [66] Carr, B., Raidal, M., Tenkanen, T., Vaskonen, V., Veermäe, H.: Primordial black hole constraints for extended mass functions. *Phys. Rev. D* **96**(2), 023514 (2017) <https://doi.org/10.1103/PhysRevD.96.023514> [arXiv:1705.05567](https://arxiv.org/abs/1705.05567) [astro-ph.CO]
- [67] Hütsi, G., Raidal, M., Vaskonen, V., Veermäe, H.: Two populations of LIGO-Virgo black holes. *JCAP* **03**, 068 (2021) <https://doi.org/10.1088/1475-7516/2021/03/068> [arXiv:2012.02786](https://arxiv.org/abs/2012.02786) [astro-ph.CO]
- [68] Abbott, R., *et al.*: Population of Merging Compact Binaries Inferred Using Gravitational Waves through GWTC-3. *Phys. Rev. X* **13**(1), 011048 (2023) <https://doi.org/10.1103/PhysRevX.13.011048> [arXiv:2111.03634](https://arxiv.org/abs/2111.03634) [astro-ph.HE]

Methods

Cooling sequence: The cold atom apparatus used in this experiment has previously been described in Refs. [38, 49]. To prepare samples of cold ^{87}Sr , the atoms are first collected for 1 s into a blue 3D magneto-optical trap (MOT) that uses the $^1\text{S}_0 \rightarrow ^1\text{P}_1$ transition at 461 nm and a field gradient of 3.5 mT cm^{-1} . Atoms that leak into the metastable $^3\text{P}_2$ manifold are recycled into the MOT using repump lasers at 679 nm and 707 nm. For efficient repumping of ^{87}Sr , frequency sidebands at 585 MHz and 487 MHz are applied to the 707 nm light using an electro-optic modulator, creating frequency components near-resonant with transitions from all five hyperfine manifolds of $^3\text{P}_2$ [50].

After the blue MOT is switched off, the atoms are captured into a red MOT operating on the $^1\text{S}_0 F = 9/2$ to $^3\text{P}_1 F' = 11/2$ transition at 689 nm, using a field gradient of $390 \mu\text{T cm}^{-1}$. Sidebands at 1463.265 MHz are applied to the 689 nm light using a resonant electro-optic modulator, addressing the $F = 9/2$ to $F' = 9/2$ transition in order to stir the atoms between Zeeman sublevels of the ground state, mitigating losses into weakly-confined sublevels [23]. During the first 120 ms in the red MOT an intensity of $1800 I_{\text{sat}}$ is used in each of the six MOT beams, where $I_{\text{sat}} = 3 \mu\text{W cm}^{-2}$ is the saturation intensity of the 689 nm transition. To capture the wide range of Doppler-shifted atoms released from the blue MOT, sawtooth-wave modulation is applied to the 689 nm light at a sweep frequency of 20 kHz and a peak-to-peak sweep range of 6.2 MHz [51]. For the following 100 ms, while in the “narrowband” red MOT, the sawtooth frequency modulation is switched off and the intensities of the six MOT beams are ramped linearly from $340 I_{\text{sat}}$ to $40 I_{\text{sat}}$. In order to help support the atoms against the force of gravity, a seventh, unbalanced MOT beam—the “up” beam—is introduced in the vertical direction during the narrowband MOT. The up beam is necessary for creating narrowband red MOTs below $100 I_{\text{sat}}$ without significant atom loss. Upon completion of the narrowband red MOT, the atoms have a temperature of $2 \mu\text{K}$ and are compressed into a region comparable in size to the optical dipole trap.

Dipole trap and state preparation: Two crossed optical dipole traps, separated vertically by 1 mm, are formed by separate 2.5 W horizontal beams at 1064 nm with horizontal and vertical $1/e^2$ radii of $220 \mu\text{m}$ and $23 \mu\text{m}$ respectively, crossed with a shared 840 mW vertical beam at 813 nm with $1/e^2$ radii of $110 \mu\text{m}$ in both transverse axes. Both dipole traps are present for the duration of the red MOT. The bias magnetic field, intensity, and detuning of the narrowband red MOT are optimised to load the atoms into the upper of the two dipole traps. To load the bottom optical dipole trap, the red MOT is released for 11 ms by switching off the 689 nm beams. During this time, the atoms already in the top trap are held in place, while the hotter atoms remaining from the narrowband red MOT fall towards the bottom trap. While the atoms fall, the vertical bias magnetic field is stepped such that the zero of the quadrupole magnetic field is close to the bottom dipole trap. After 11 ms of free fall, the red MOT beams are switched back on for 20 ms, gathering the fallen atoms into a MOT centered on the bottom dipole trap, while heating half of the atoms out of the top trap by off-resonant scatter.

After both dipole traps are loaded, the MOT beams are switched off, a horizontal bias field is applied, and the trapped atoms are optically pumped into the stretched

state $M_F = 9/2$ by applying a horizontal bias field of 38 μT and delivering a 20 ms pulse of circularly-polarised light at 689 nm, resonant with the $^1\text{S}_0 F = 9/2$ to $^3\text{P}_1 F' = 9/2$ transition. During the optical pumping, sawtooth-wave frequency modulation is applied to the 689 nm light at a rate of 30 kHz over a range of 6 MHz. Finally, all beams except the dipole trap are switched off, and the bias magnetic field is adiabatically ramped to the final field used for atom interferometry: 31 μT aligned with the linear polarisation of the vertical 698 nm clock beam.

Velocity selection on the clock transition: The clock beam at 698 nm propagates vertically upward through both dipole trap regions with a waist of 600 μm . The clock laser linewidth is verified against an independent cavity-stabilised laser as below 2 Hz, prior to delivery of the light to atoms through an uncompensated 10 m fibre. Clock spectroscopy sequences are carried out immediately after atoms are released from both dipole traps, and then the excitation fraction is detected using a 50 μs fluorescence pulse at 461 nm to detect the atom number in the ground state $^1\text{S}_0$, followed by a 3.5 ms repumping pulse at 679 nm and 707 nm and another 50 μs fluorescence pulse at 461 nm to detect atoms that are in the $^3\text{P}_0$ state after the interferometry sequence. Scattered light from each 461 nm spectroscopy pulse is gathered in separate exposures on an *Andor iXon Ultra 897* EMCCD camera, and a separate EMCCD image without atoms present is used to subtract background counts.

At the maximum available clock power of 640 mW, a Rabi π -pulse time of 40 μs is measured. However, the clock transition is observed to have a peak excitation fraction of 0.3, and a Doppler-broadened linewidth of 60 kHz—considerably larger than the 20 kHz Fourier limit. In order to improve the fidelity of the Rabi pulses in the atom interferometer sequence, a velocity selection procedure is used. The clock beam is pulsed on for 200 μs at 20 mW, implementing a π pulse that excites the slowest atoms to the upper clock state $^3\text{P}_0$. The atoms in the ground state are then pushed away using a 500 μs pulse at 461 nm, leaving only the slow atoms in the $^3\text{P}_0$ state to enter the interferometry sequence.

Clock atom interferometry: The clock atom interferometry consists of a sequence of three resonant pulses on the 698 nm clock transition, with pulse areas $\pi/2 - \pi - \pi/2$, a π pulse time of $t_\pi = 44 \mu\text{s}$, and a dark time of $T = 100 \mu\text{s}$ between each consecutive pulse. For the data in Figure 4, the phase of the clock light is always stepped deterministically during the dark times such that the phase of the first, second and third pulses are 0, ϕ and 4ϕ respectively, with ϕ ranging from 0 to 2π in 100 steps in a randomized order. Each datapoint in the right-hand side of Figure 4 results from 2×100 samples, interleaved between “High Laser Noise” and “Low Laser Noise” samples. “High Laser Noise” samples have additional phase steps applied during the interferometer dark times (see Figure 3), drawn independently from a Gaussian distribution with a standard deviation of 4π rad and mean of 0 rad. This phase randomisation mimics a realistic scenario for the laser phase noise that would likely be present in a very long-baseline atom interferometer, in which the long dark time will result in significant accumulated phase in the clock laser local oscillator (see below). The phase randomisation fully masks the fringes in each individual interferometer, but does not affect the measurement of the relative phase of the two interferometers.

Laser phase noise estimate for a km-scale detector: The phase noise imparted onto the atoms by the laser can generally be calculated from the spectral density of frequency fluctuations on the laser [52]. In our prototype, the laser phase imprinted on each atom interferometer in one repetition of the interferometer sequence beginning at time t is approximately $\phi_{\text{laser}} = \varphi(t) - 2\varphi(t+T) + \varphi(t+2T)$, where $\varphi(t)$ is the time-dependent phase of the laser field oscillating as $\cos(kz - \omega_0 t + \varphi(t))$, and where the approximation holds in the limit of short beamsplitter and mirror pulses separated by a dark time T [34]. Treating $\varphi(t)$ as a stationary noise process with one-sided power spectral density $S_\varphi(f)$, and applying the optical Wiener-Khinchin theorem [53], we observe a variance in interferometer laser phase:

$$\begin{aligned} \langle \phi_{\text{laser}}^2 \rangle &= \langle (\varphi(t) - 2\varphi(t+T) + \varphi(t+2T))^2 \rangle \\ &= 6 \langle \varphi(t)\varphi(t) \rangle - 8 \langle \varphi(t)\varphi(t+T) \rangle + 2 \langle \varphi(t)\varphi(t+2T) \rangle \\ &= \int_0^\infty S_\varphi(f) [6 - 8 \cos(2\pi fT) + 2 \cos(4\pi fT)] df \end{aligned}$$

For a future long-baseline atom interferometer, we consider a model for the clock laser as a thermal-noise-limited, cavity-stabilised laser [54], with a flicker frequency noise spectrum of the form $S_\varphi(f) = S_\varphi(1 \text{ Hz})/f^3$. Propagating this functional form through the above equation, the standard deviation of the interferometer laser phase simplifies as $\sqrt{\langle \phi_{\text{laser}}^2 \rangle} = 4\pi T \sqrt{\ln(2)} \sqrt{S_\varphi(1 \text{ Hz})}$. To provide an optimistic numerical estimate of the laser phase, we assume a laser noise spectrum at the limit of current laser technology, with fractional frequency noise $S_y(f) = (10^{-33}/f)/\text{Hz}$ [55]. For the ^{87}Sr clock transition at 698 nm, the corresponding noise spectral density of clock laser phase fluctuations would be $\sqrt{S_\varphi(1 \text{ Hz})} = 14 \text{ mrad}/\sqrt{\text{Hz}}$, resulting in a standard deviation in interferometer laser phase $\sqrt{\langle \phi_{\text{laser}}^2 \rangle} = 730 \text{ mrad}$ for $T = 5 \text{ s}$, the interferometer time projected for a km-scale detector [11]. Even for an interferometer repetition rate of several shots per second, the laser phase noise imprinted on each individual interferometer is therefore far above the level needed to reach the ultimate target phase resolution of $10^{-5} \text{ rad}/\sqrt{\text{Hz}}$ [11], highlighting the need for laser noise cancellation in the differential phase $\delta\phi$.

Compounding the requirements for laser phase noise cancellation, a large momentum transfer of $n \sim 10^4$ photon recoils is targeted for long-baseline detectors [11], enhancing the detector sensitivity but imprinting laser phase noise n times onto each atom interferometer [34]. Taking into account the large momentum transfer, long-baseline interferometers are likely to be in the fully phase-randomised regime explored by the ‘‘High Laser Noise’’ dataset in this work.

Differential bias phase: In order to induce a consistent relative phase offset between the top and bottom atom interferometers, an additional, horizontal 689 nm Stark shifting pulse is applied to the top interferometer only, for 30 μs during the gap between the first $\pi/2$ -pulse and the middle π -pulse. The Stark shifting beam is detuned by -80 MHz from the $^1\text{S}_0 \ F = 9/2$ to $^3\text{P}_1 \ F' = 11/2$ transition, with a waist of 500 μm and a power of 1 mW, inducing a phase shift specifically on atoms in the ground state (the lower arm) of the top interferometer. For the data in this paper,

the Stark shifting pulse is used to generate a bias differential phase between the top and bottom interferometers, causing the data to lie on a Lissajous ellipse rather than a straight line, enabling the fit errors to be reduced [43]. In a long-baseline detector, the dark matter or gravitational wave signal would induce fluctuations in the ellipse fit angle, on top of the static bias.

Experimental control: Electronic control signals are produced through the FPGA-based experimental control platform ARTIQ [56]. Control software is written in Python and is available open-source at Ref. [57].

Phase extraction: To extract the differential phase from datasets, a normalized excitation fraction is calculated using the three fluorescence images for both the top and bottom interferometers, with images corresponding to (1) the ground-state population, (2) the excited state population, and (3) the background scatter. A series of least-squares fits are then performed of an elliptical conic section to bins of 100 consecutive excitation fraction measurements, with the excitation fraction of the bottom (top) interferometer plotted on the x (y) axis. This series of ellipse fits results in a time-series of differential phases $\delta\phi(t_i)$. This method is vulnerable to systematic error [43] when $\delta\phi \approx 0$ so we set our bias phase ϕ_{Stark} to $\sim 62^\circ$ to avoid this, simplifying our analysis.

Data filtering: The 461 nm, 689 nm, and 698 nm laser locks are monitored throughout the experiment. Experiment runs in which one or more of these locks fails are considered invalid and excluded from the data. As the 698 nm lock is only polled every 10 s, longer than the duration of a single shot (~ 3 s), all affected shots are discarded. Typically, a failure in the 461 nm or 689 nm locks results in reduced atom number, while a loss of the 698 nm lock affects the excitation fraction.

Atom numbers: Atoms are detected at the end of atom interferometry sequences through fluorescence imaging on an EMCCD camera. Under the assumption that fluorescence scales linearly with atom number, the fluorescence signal can be converted to atom number using a calibration derived from absorption imaging of clouds of atoms prepared under identical conditions as those used for the atom interferometry. The atom number N in the calibration dataset is extracted from the raw absorption images through the relation $N\sigma(\omega_{\text{cal}}) = \int OD(x, y) dx dy$ [58], where $OD(x, y)$ is the optical depth of the sample at transverse position x, y in the absorption probe beam, and $\sigma(\omega_{\text{cal}})$ is the absorption cross-section of the ^{87}Sr atoms at the laser frequency ω_{cal} used during the calibration dataset.

Since the hyperfine shifts of the states $^1\text{P}_1$ $F = 7/2, 9/2$, and $11/2$ are respectively +37, -23, and -6 MHz [59], which are significant compared with the 30.5 MHz natural linewidth of the $^1\text{P}_1$ state [60], the absorption cross-section $\sigma(\omega)$ in ^{87}Sr is generally polarisation- and M_F -dependent. To avoid reliance on direct measurements of the polarization of our absorption probe light and the M_F state of the atoms, we instead measure the relative absorption amplitudes of the three lines from $^1\text{S}_0$ to $^1\text{P}_1$ $F = 7/2, 9/2$, and $11/2$ by carrying out spectroscopy over a ± 100 MHz range of detunings, using samples of atoms pumped into $M_F = 9/2$ using the same preparation sequence as for the atom number calibration and the atom interferometry datasets. We fit the peak amplitudes $\sigma_{7/2}$, $\sigma_{9/2}$, and $\sigma_{11/2}$ of the three Lorentzians to the absorption

spectroscopy data, using fixed literature values for the linewidths and the hyperfine splittings between the Lorentzians [59, 60]. The relative amplitudes of the three Lorentzians can be converted into a calibrated cross-section function $\sigma(\omega)$ by normalising the amplitudes such that the sum of the peak absorption cross-sections matches the resonant absorption cross-section for the simpler isotopes with zero nuclear spin, i.e. $\sum_F \sigma_F = \sigma_0 = 3\lambda^2/2\pi$ [58]. Based on these Lorentzian fits, the implied absorption cross-section for the 461 nm laser frequency ω_{cal} used during the atom number calibration dataset is $\sigma(\omega_{\text{cal}}) = 0.68(7)\sigma_0$. We obtain a total atom number uncertainty of 10 % during the atom interferometry dataset, dominated by the uncertainty in the absorption cross-section $\sigma(\omega_{\text{cal}})$ due predominately to drifts in the 461 nm laser frequency.

The mean atom number in the top trap was 1280(130) atoms and in the bottom 1600(160) atoms. Due to a drift in the 689 nm laser frequency, the atom number in each trap drifted approximately linearly across the dataset, at a rate of ~ -42 atoms per hour in the top trap and ~ 8 atoms per hour in the bottom trap. This drift is predominantly due to the drift in the ultralow expansion glass reference cavity, and could be compensated in future experiments by employing a feed-forward signal on the laser frequency. No significant difference in atom number was observed between shots with and without induced phase noise.

Extraction of noise levels: To estimate any additional noise σ_L in our measurement of $\delta\phi$ caused by injecting laser noise, we model the time-series of extracted phases as

$$\delta\phi(t_i) = \mathcal{N}(\delta\phi_0, \sigma_{\delta\phi}) + \alpha t_i \quad ,$$

where $\mathcal{N}(\mu, \sigma)$ represents a random variable that is normally distributed with mean μ and standard deviation σ . We use a No-U Turn Markov-chain Monte-Carlo method implemented using the PyMC package [61] to sample from the posterior distribution of $\sigma_{\delta\phi}$ for the LLN and HLN datasets, reporting the 68 % credible intervals of the posterior distributions as $\sigma_{\text{LLN}} = 7.80^{+0.46}_{-0.59}$ mrad and $\sigma_{\text{HLN}} = 8.27^{+0.45}_{-0.64}$ mrad.

We find a linear drift in both datasets of $\alpha = 3.3 \times 10^{-7} \text{ rad s}^{-1}$ which we ascribe to the known drift of our 698 nm clock laser of 0.1 Hz s^{-1} , which alters the velocity class of atoms selected by the state-preparing velocity selection pulse. Since the atoms' velocities and locations are strongly correlated after release from their confining dipole traps, this would lead to a small movement within the Stark shifting beam and therefore a variation in the applied phase shift ϕ_{Stark} . This small drift does not affect our ability to compare the LLN and HLN datasets, since both datasets were interleaved shot-to-shot and experienced the same drift.

Estimation of Standard Quantum Limit: To estimate the SQL, a Monte Carlo simulation was performed generating 10^3 synthetic datasets with variation in atom number consistent with the uncertainty in mean from the absorption method described above, known shot-to-shot variation within datasets, and zero additional noise sources. Each dataset consisted of 10^5 simulated interferometer shots, each of which experiences contrasts of 0.81 and 0.84 for the two traps, and mean atom numbers of 1280(130) and 1600(160) respectively, matching our real data. These datapoints were binned into sets of 100 and an ellipse was fitted to each bin, producing a time-series of differential phases $\delta\phi$. The standard deviation of these time-series is the simulated SQL noise level

σ_{SQL} — their distribution provides an uncertainty due to variation in atom number, the 68 % credible interval of which is $\sigma_{\text{SQL}} = 7.7(3) \text{ mrad}$, shown in Figure 4d.

Code availability: Python code and raw data for the results presented in this work are available at Ref. [57].

Gravitational Wave Detection Prospects: In Figure 1, the outlined regions show the expected sensitivities of the indicated gravitational wave detectors at a signal-to-noise ratio $\text{SNR} \geq 8$ from the final stages of equal mass black hole mergers, after the binaries come within the innermost stable circular orbit, during one year of operation. The detector sensitivities are taken from [2, 5, 17, 62]. The sensitivity of the AION-km detector incorporates an estimate of the possible mitigation of gravity gradient noise based on [63, 64]. The cyan symbols are simulated GW signals from black hole mergers based on a model of hierarchical assembly of supermassive black holes starting from $100M_{\odot}$ black hole seeds at redshift $z = 20$ that could be the remnants of collapsed first-generation Population III stars. This scenario is consistent with JWST and other observations of supermassive black holes [6] and predicts $\sim 10^3$ AION-km detections per year. Scenarios with (an admixture of) heavier seeds and fewer detections are also consistent with the current supermassive black hole data. The violet dots are GW signals from mergers [65] of a hypothetical population of primordial black holes computed assuming a primordial black hole (PBH) population that comprises 0.2% of all the dark matter and has a log-normal mass distribution $\psi(M) \propto \exp\left(-\frac{\ln^2(M/M_c)}{2\sigma^2}\right)$ with a mean $M_c = 10M_{\odot}$ and width $\sigma = 3$, which is consistent with the available constraints [66]. The yellow dots are GW signals from a sample of stellar mass black hole mergers assuming a truncated power-law mass function in the mass range from $3M_{\odot}$ to $60M_{\odot}$ and a merger rate that follows the star formation rate, peaking around $z = 2.5$ [67, 68]. The exponent and the amplitude are fixed by fitting the data of [2–4].